Preprint Notice

⚠ This manuscript is a preprint and has not been certified by peer review.

It has been made publicly available via Zenodo to facilitate early dissemination and feedback. The final version of this work may differ after peer review.

This manuscript is intended for submission to Magnetic Resonance in Medicine (MRM).

Preprint DOI: https://doi.org/10.5281/zenodo.15063820.

Automatic determination of glymphatic flow with the DTI-ALPS-index along the principal axis system in native imaging space corrects for head and fibre orientation

Ali Ajouz,[1,2,3] Olav Jansen,[1] Lynn Johann Frohwein,[3] Svea Seehafer,[1] Naomi Larsen,[1] and Jan-Bernd Hövener[1,2*]

[1] Department of Radiology and Neuroradiology, UKSH, CAU Kiel, Kiel, Germany.
[2] Department of Radiology and Neuroradiology, SBMI, CAU Kiel, Kiel, Germany.
[3] Siemens Healthineers AG, Forchheim, Germany.

Corresponding author: Jan-Bernd Hövener; Mail: jan.hoevener@rad.uni-kiel.de

Abstract

Keywords: Neurofluids**,** DTI-ALPS-index, glymphatic system, brain clearance, image registration

Purpose: This work aims to decrease the dependence of the DTI-ALPS-index on the head and fibre orientation, calculating the DTI-ALPS-index along the principal diffusion directions. It is investigated if an automated ROI placement could lead to a more robust DTI-ALPS-index without native data registration.

Methods: We calculated the DTI-ALPS-index along the principal diffusion directions (ALPS-PAS) and compared it with the original DTI-ALPS-index along the scanner's laboratory frame (ALPS-LAB) using simulation and in vivo measurements.

To calculate the DTI-ALPS-index in native space, we developed a novel calculation algorithm for an automatic ROI placement technique and compared it to a manual ROI placement and existing atlas-based ROI placement. Further, a whole-brain DTI-ALPS-map was introduced.

Results: Simulations demonstrated the dependence of the DTI-ALPS-index on the head and fibre orientation and the in vivo measurements yielded higher ALPS-PAS than ALPS-LAB. The novel ROI placement led to a more robust DTI-ALPS-index evaluation in meaningful regions than the manual ROI placement. The DTI-ALPS-map indicated an anisotropy between the second and third principal diffusion direction in other brain areas besides the ALPS-fibre-regions.

Conclusion: ALPS-PAS eliminates the head and fibre orientation dependence, which enables the calculation in the native data space without registration of the acquired data. The automatic ROI placement reduces the operator dependent ROI selection, which could be beneficial for longitudinal studies.

Introduction

The clearance of metabolic waste and solute transport are essential for maintaining proper brain function[1]. Evidence suggests that this process is facilitated by a glial lymphatic (glymphatic) system, though it remains difficult to identify both in vivo and through histological analysis. Metabolic waste primarily originates from neuronal activity, including byproducts of neurotransmitter metabolism, misfolded proteins, and the breakdown of cellular components[1,2].

It was suggested that the glymphatic system operates within the perivascular space (PVS), where aquaporin-4 (AQP4) channels support water exchange with the brain parenchyma, clearing solutes and proteins such as amyloid-beta[3].

Several MRI based methods were suggested to investigate selected aspects of this system[4]. These include methods with[5] and without Gadolinium-based contrast agents (GdCA). While GdCA methods allow tracking the pathway of a molecule (the Gd-complexes) for minutes to hours with comparably high signals, the ability of GdCA to probe AQP4 channels is unclear[1]. Methods without GdCA, on the other hand, image water molecules, but may suffer from less signal and a shorter observation window (for example arterial spin labeling (ASL)[6], chemical exchange saturation transfer (CEST)[7], intravoxel incoherent motion (IVIM)[8] , and diffusion tensor imaging along the perivascular space (DTI-ALPS-index)[9–11].

The latter found that in a specific brain area, the diffusion (or slow flow) of water molecules perpendicular to the dominant direction of neuronal fibres is anisotropic. It was shown that the diffusion weighted signal perpendicular to the dominant fibre orientation, along the postulated microvasculature, was weaker than the diffusion weighted signal perpendicular to the dominant fibre orientation and perpendicular to the microvasculature, for example by 40% in healthy controls[9]. This anisotropy was found to decrease with dementia and age[9], suggesting that this "flow" decreases with these factors.

These results may suggest a glymphatic flow along the perivascular spaces (ALPS) in selected areas of the human brain. The original and current implementations of DTI-ALPS-index often use the diffusion in the Cartesian directions of the laboratory frame (LAB) to determine the index (or flow). However, the laboratory frame (defined by the physical orientation of the gradient coils) is not necessarily aligned with the nerve fibres in the brain. Head and fibre orientation will affect the diffusion metrics[9] and thus the DTI-ALPS-index.

Different head orientation may be addressed by transforming the measured data to a standard head orientation, but requires heavy processing[12,13] and does not account for individual fibre orientations (for example the FMRIB58 template in Montreal Neurological Institute (MNI) space). A method to calculate the DTI-ALPS-index in the untransformed patient space, while correcting for the head orientation and taking the fibre orientation into account, however, was not reported.

Here, we propose to measure the anisotropy with respect to the main fibre orientation instead of the Cartesian coordinates of the scanner. We determined the main fibre orientation by calculating the main diffusion directions in a principal axis system (PAS)[14,15] (Figure 1B) and calculated the DTI-ALPS-index accordingly.

Another key factor to determine the DTI-ALPS-index reliably is the (reproducible and precise) selection of the region where the index is calculated. Transforming the acquired data to an atlas with preselected regions[13] involves non-rigid transformations with many degrees of freedom and strongly affects the measured MRI data[16] (Figure 1C). Here, we propose to calculate DTI-ALPS-index in regions defined on an atlas and transferred to the measured images. Thus, we developed an

atlas-based method to automatically select regions on the acquired data, calculated the DTI-ALPS-index both in the LAB and in the PAS, and compared it to the values obtained in an atlas space. We hypothesized that these methods a) increase the DTI-ALPS-index and b) reduce the variability.

Methods

DTI-ALPS-index computation

The diffusion tensor $\widehat{D}$ can be described in the LAB of an MRI-scanner as

$$\widehat{D} = \begin{bmatrix} D_{xx} & D_{xy} & D_{zz} \\ D_{yx} & D_{yy} & D_{yz} \\ D_{zx} & D_{zy} & D_{zz} \end{bmatrix}, \quad (1)$$

where x, y and z are the indices of the diffusion coefficients and refer to the Cartesian coordinates of the scanners' gradients. In this frame of reference (LAB), the DTI-ALPS-index (ALPS-LAB) was introduced in Ref.[9] as (Figure 1A):

$$\text{ALPS-LAB} = \frac{\overline{Dxx,proj,Dxx,assoc}}{\overline{Dyy,proj,Dzz,assoc}}, \quad (2)$$

where *proj* describes the *superior corona radiata* (SCR) region in the brain where projection fibres are dominant, and *assoc* describes the *superior longitudinal fasciculus* (SLF) region in the brain where association fibres are dominant. SCR and SLF refer to the ALPS-fibre-regions.

Diagonalising $\widehat{D}$ yields $\hat{\Lambda}$, which translates to a transformation of the coordinate system, resulting in the principal axis system (PAS) or principal diffusion directions as the eigen basis of the new coordinate system[17]. $\hat{\Lambda}$ is defined as

$$\hat{\Lambda} = \begin{bmatrix} \lambda_1 & 0 & 0 \\ 0 & \lambda_2 & 0 \\ 0 & 0 & \lambda_3 \end{bmatrix}, \quad (3)$$

where the eigenvalues of $\widehat{D}$ are in the corresponding order: $\lambda_1 \geq \lambda_2 \geq \lambda_3$ (Figure 1B). The diagonalised matrix is used to calculate ALPS-PAS[14,15]:

$$\text{ALPS-PAS} = \frac{\overline{\lambda x,proj,\lambda x,assoc}}{\overline{\lambda y,proj,\lambda z,assoc}}, \quad (4)$$

where λ_x is λ_2 or λ_3 depending on whose eigenvector has the larger x component, and λ_y is the remaining λ_2 or λ_3 (note that λ_1 is the main diffusion direction along

the dominant fibres and not used to calculate ALPS-PAS). In the ALPS-LAB and ALPS-PAS calculations, the diffusion coefficients (D_{xx}, D_{yy} *and* D_{zz}) or, in PAS (λ_1, λ_2 *and* λ_3) are selected from the tensors in the voxels of the ROIs described later in this chapter. The overbars indicate the averages.

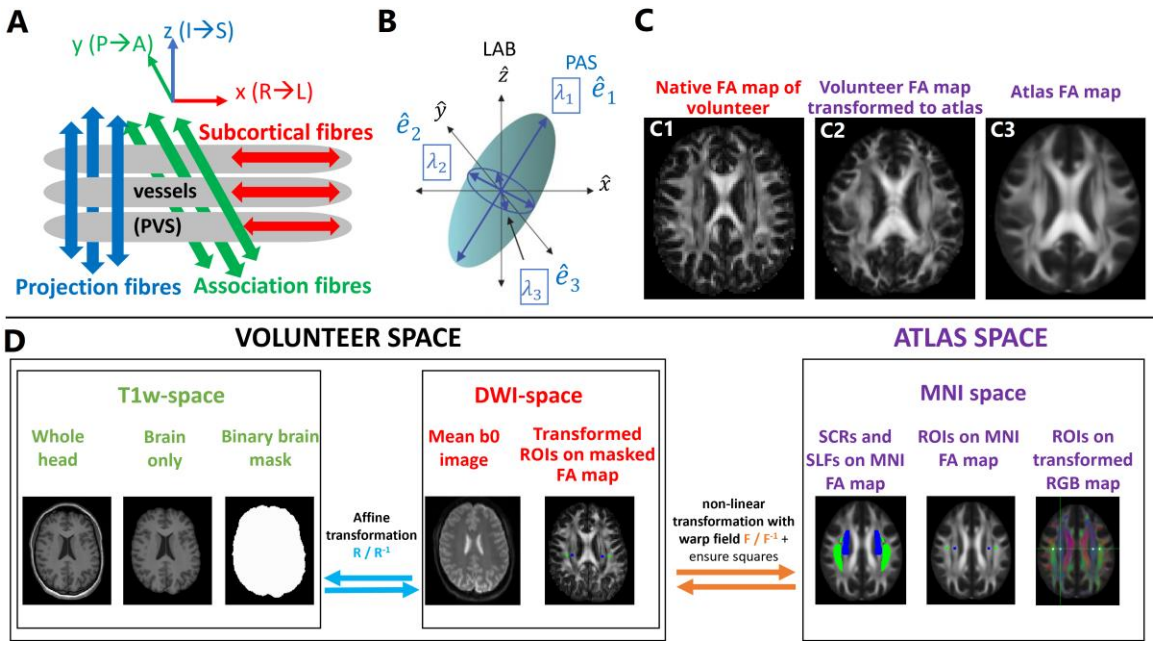

Figure 1: (A) Idealized scheme of the vasculature (grey) in the projection (blue), association (green) and subcortical (red) fibre area. In classical ALPS-LAB, the directions of these fibres are assumed to coincide with the Cartesian coordinate system in the laboratory frame of reference ($\hat{x}, \hat{y}, \hat{z}$). (B) Analysing the diffusion tensor shows that its principal components ($\hat{e}1, \hat{e}2, \hat{e}3$) do not necessarily align with the Cartesian system.
(C1) Native fractional anisotropy (FA) map of the volunteer, (C2) after transformation into the space of an atlas (MNI152, FMRIB58), which is shown in (C3). Note how strongly the features between C1 and C2 changed.
(D) Schematic view of the workflow used for the automatic evaluation of ALPS-LAB and ALPS-PAS in the volunteer DWI and atlas MNI spaces. In volunteer space, the matrix R/R^{-1} was used to transform the brain mask from T1w space to DWI space. The matrix F / F^{-1} was used to transform between the volunteer DWI and atlas MNI space. Four volumes of size 4x4x4 mm^3 in the SCR and SLF were selected in the MNI space.

Simulation experiments and Kardan-angles

We performed simulations, to investigate, how strongly ALPS-LAB is affected by a mismatch between fibre and gradient orientation. We assumed a diffusion tensor $\widehat{D}$ of the projection area diagonal in the laboratory frame with its eigenvalues: 1.7, 0.4,

0.2 μm²/ms. We applied selected rotations to the coordinate system of $\widehat{D}$ (rotations of individual or all axes, defined by Kardan-angles (Ψ, Θ, Φ)[18] for the intrinsic rotation (ZY'X''), Supporting Figure S1.1, Supporting Figure S1.3) and calculated ALPS-LAB. Note, for the simulation, we created one tensor in one voxel. Therefore, we calculated ALPS-PAS by dividing the second eigenvalue by the third for ALPS-PAS and D_{xx} by D_{yy} of one tensor only. For ALPS-LAB, we always divided D_{xx} by D_{yy}, as the simulated initial tensor has an orientation like the tensors of the projection fibres.

Without rotation, ALPS-LAB is "ideal" and identical to ALPS-PAS. We used the ratio of ALPS-LAB / ALPS-PAS to assess the similarity of both indices.

In vivo experiments

In vivo measurements were acquired at 3T (MAGNETOM Cima.X scanner, Siemens Healthineers AG, Forchheim, Germany) with a maximal gradient amplitude of 200 mT/m, a maximum slew rate of 200 T/m/s and a two-channel body transmit coil, and 64-channel receive head neck coil. Using a slice selective, diffusion weighted gradient echo sequence with EPI readout, 66 diffusion volumes (b = [0,1000] s/mm², diffusion gradient directions = [6, 30], averages = [1, 2]) plus six b = 0 s/mm² images with reversed phase encoding direction were acquired (FOV = 220 x 220 mm², 50 slices with 2 mm thickness, 2 mm isotropic resolution, matrix size 110x110x50, TE = 41 ms, volume TR = 6600 ms, readout bandwidth = 1698 Hz/Px, flip angle = 90°, GRAPPA (factor 2, 28 reference lines), phase partial Fourier 0.75, effective echo spacing = 0.3 ms). In addition, a 3D T1-weighted (T1w) MP-RAGE image was acquired (FOV = 256 x 256 x 192 mm³, 1 mm isotropic resolution, TE = 2.45 ms, TR = 1900 ms).

The protocol was applied to nine healthy subjects (age: 23-49, six females and three males, Supporting Table S1). Test-retest measurements were conducted on two subjects (3, 9) with a five-minute break in between. Subject one was measured with and without deliberate head rotation to the top-right hand corner.

Image processing

T1w images were corrected for bias fields, denoised and used to generate a brain mask (ANTs[19], Figure 1D). DWI post-processing included denoising, unringing (Mrtrix[20]), distortion and eddy current corrections (FSL[16]). A transformation matrix R between T1w and DWI images was calculated and used to transform the brain mask to the DWI data (Epireg, Vecreg)[16]. The diffusion tensor and color-coded FA (RGB) maps (Dipy[21]) were calculated on the masked diffusion data.

In addition, the brain-masked DWI data was transformed to the MNI atlas space by calculating a transformation matrix F using the FA maps of both spaces with linear and non-linear transformations (flirt and fnirt)[16].

ROIs

We calculated ALPS-LAB and ALPS-PAS for the left and the right hemisphere by creating ROIs in the ALPS-fibre-regions in three different ways. All ROIs have the same volume (4x4x4 mm^3). For each way, four ROIs were defined, with one ROI in each ALPS-fibre-region. This resulted in two ROIs per hemisphere: one in the SCR and one in the SLF, on both the left and right sides (Figure 1D).

A) MNI ROIs: The four ROIs were placed on a brain template (FMRIB58_FA_1mm, MNI152 space[22–24]) (existing atlas based automated way[13]).
B) Manual ROIs in DWI space: An experienced radiologist selected the ROIs manually on the volunteer RGB maps (the way DTI-ALPS-index was introduced[9]).
C) MNI ROIs in DWI space: the MNI-ROIs from A) were transformed to the DWI space using F^{-1} by a custom algorithm, which was applied to retain the structural integrity of the ROIs. This algorithm ensures that the ROIs remain square, with a voxel size of 2x2x2 voxels (corresponding to 4x4x4 mm^3). If transformation results in more than two voxels in a given direction, the two voxels with the highest intensity are retained. If only one voxel remains, the missing voxel is determined by selecting the neighbouring voxel with the highest FA value (novel technique of this work).

In the following, the ROIs defined by the three different ROI placements 'MNI ROIs', 'Manual ROIs in DWI space' and 'MNI ROIs in DWI space' are referred to as 'ROI-options'.

For each subject and in each of the four ALPS-fibre-regions, the individual distance between the centres of mass (Δ) for ROI-options B and C in DWI space was calculated, followed by the mean and standard deviation across subjects.

Angles and ALPS-LAB/ ALPS-PAS

The orientation of the diffusion tensor was described by intrinsic Kardan-angle rotations for each ROI-voxel and as mean of all voxels in one ROI (ZY'X'' with the angles Ψ, Θ, Φ, Supporting Figure S1.1, Supporting Figure S1.3).

Similarly, the absolute angles between the laboratory axes and the principal axes of the diffusion tensors were calculated (Supporting Figure S1.2).

ALPS-LAB and ALPS-PAS were calculated for each subject and each hemisphere (Equation 2, Equation 4), for all ROI-options.

Statistical evaluation

The mean ALPS-LAB/ ALPS-PAS and relative standard deviation (coefficient of variance, CV) was computed for all subjects and all ROI-options (A, B, C).

Two paired t-tests enabled a comparison of ALPS-LAB and ALPS-PAS for each ROI-option independently. To increase test validity, indices of both brain hemispheres were combined (significance $p = 0.05$; two-sided and one-sided (alternative hypothesis H_1: ALPS-LAB<ALPS-PAS)).

ALPS-maps

To generate a map of ALPS-LAB and ALPS-PAS of the entire brain, the indices were calculated for each voxel where FA was unequal to zero. Instead of comparing the diffusivity of ROIs placed in the two ALPS-fibre-regions, the second and third largest diffusion components within one voxel were used, similar to the simulated tensor above.

The ALPS-PAS-map was computed with ALPS-PAS-voxel = λ_2 / λ_3- 1 and the ALPS-LAB-map assigned D_{xx}, D_{yy} and D_{zz} to D_a, D_b and D_c where $D_a > D_b > D_c$ and therefore ALPS-LAB-voxel = D_b/D_c-1.

Results

The effect of a misalignment of the brain anatomy (i.e. the fibre and hypothetical PVS orientation) to the coordinate system of the scanner was evaluated by simulations.

As expected, the DTI-ALPS-index was found to depend on the relation of both systems.

For example, a mean deviation of all three angles by ±5° to ±10° resulted in at least 5% and a maximum 20% change of the DTI-ALPS-index (it means that ALPS-PAS differs at least 5% and maximum 20% from ALPS-LAB) (Figure 2.1).

Assuming a single Ψ = ±20° rotation around the Z-axis resulted in an DTI-ALPS-index decrease of 20% (Figure 2.2). The strongest effect was found for a misalignment of the Y'-axis (Φ rotation around the novel Y'-axis), where ±20° rotation resulted in 45% decreased DTI-ALPS-index.

The ratio of ALPS-LAB / ALPS-PAS simulated for the total range of Kardan-angles is provided in the supporting information (Supporting Figure S2 A, B).

These data suggest that small rotations of the head or individual fibres are likely to affect the DTI-ALPS-index.

Regarding the in vivo measurements, maximum Kardan-angles of ±35° were observed for individual voxels, and ±15° for the ROI average (Figure 2.3).

Thus, a significant deviation between the Cartesian directions of the laboratory frame and the principal diffusion directions was found in vivo (Supporting Figure S1). The magnitude of the deviations suggests that this effect can increase the measured in vivo DTI-ALPS-index up to 20%.

A more intuitive understanding of these rotations is obtained when the absolute angle between the Cartesian axis and the new principal axis is evaluated (Supporting Figure S3).

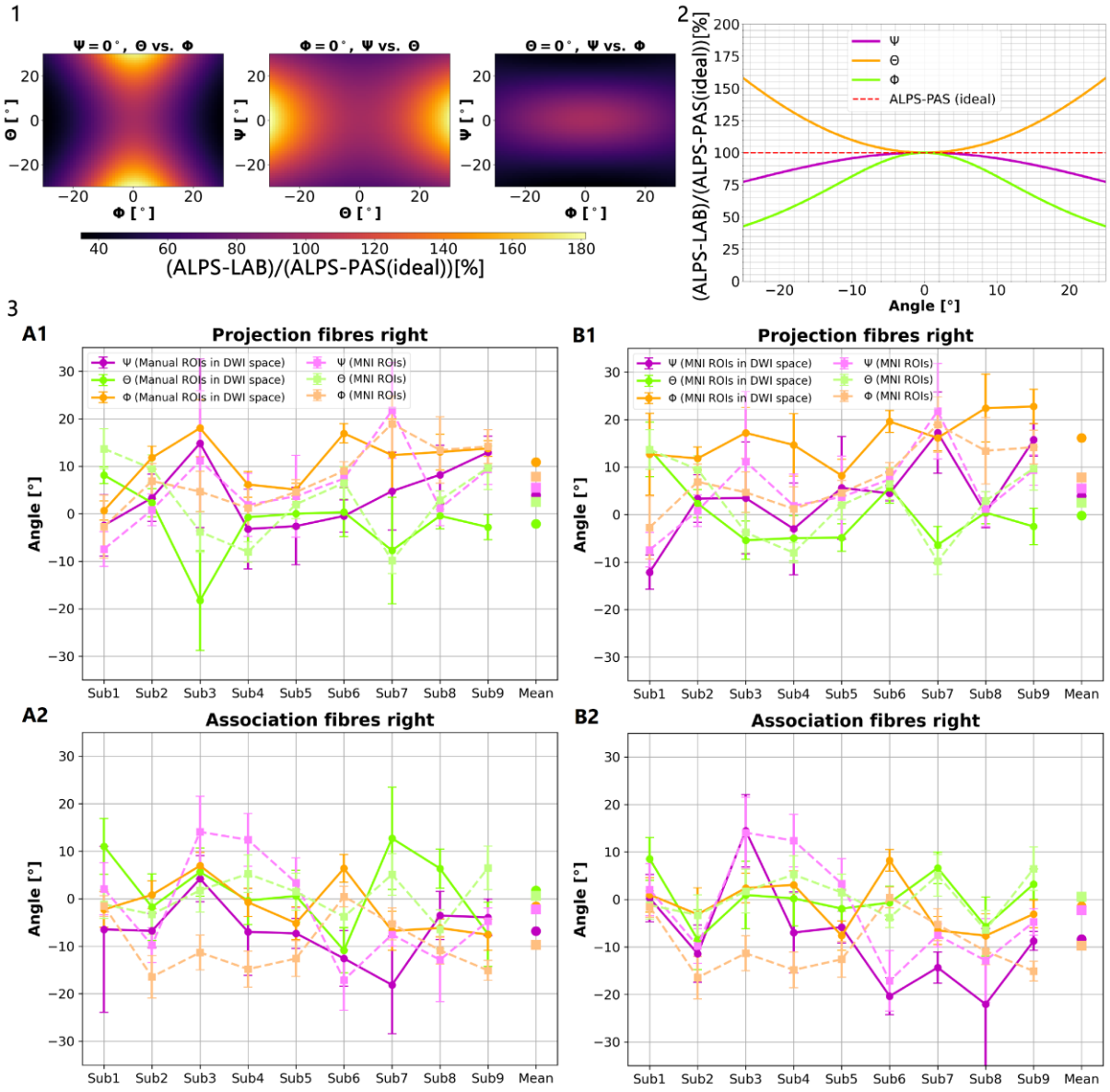

Figure 2: (1) Effect of rotations on the DTI-ALPS-index. Three simulated Kardan-angle combinations; in each subfigure one angle is set to zero whereas the other two are simulated for a selected Kardan-angle range. (2) Similar to (1) but setting two Kardan-angles to zero while varying the third in the same angle range. (3) The curves represent the mean and standard deviation values of the three Kardan-angles computed for each voxel within the ROIs, which are defined per ALPS-fibre-region. For each angle, the mean and standard deviation were calculated across voxels within each ROI for each subject. Subsequently, these values were averaged across subjects. The results shown are for the right hemisphere as an illustration. The colours violet, chartreuse and orange characterize $(\boldsymbol{\psi}, \boldsymbol{\theta}, \boldsymbol{\phi})$ in DWI space (A1,2: Manual ROIs in DWI space; B1,2: MNI ROIs in DWI space) and light violet, light chartreuse and light orange characterize $(\boldsymbol{\psi}, \boldsymbol{\theta}, \boldsymbol{\phi})$ in MNI space (MNI ROIs).

Next, ALPS-PAS and ALPS-LAB were calculated for all ROI-options (A, B, C) on the in vivo data and analysed.

Comparing ALPS-PAS and ALPS-LAB, we found that the mean ALPS-PAS was higher and statistically different than ALPS-LAB for all ROI-options, on average by 13% in the left hemisphere and 6% in the right hemisphere, and $p < 5 \cdot 10^{-6}$ (Figure 3.1, Figure 3.2A, Supporting Table S1). The CV was similar for ALPS-LAB and ALPS-PAS, with a tendency for less variance in the laboratory frame.

1

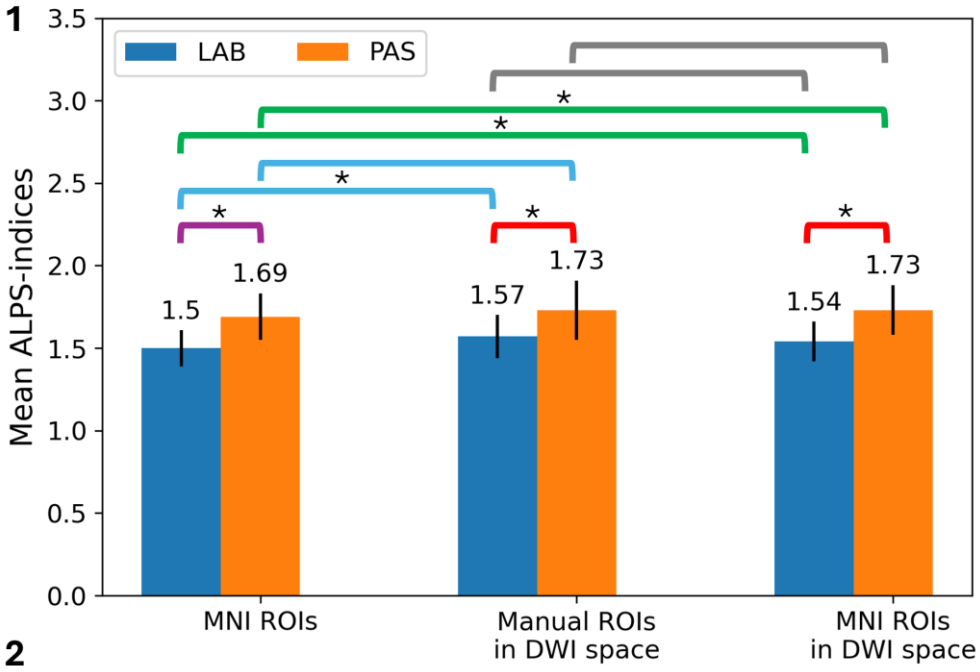

2

(A)	ALPS-LAB – ALPS-PAS		
paired t-test	**MNI ROIs**	**Manual ROIs in DWI space**	**MNI ROIs in DWI space**
two-sided test	$1.77 \cdot 10^{-7}$(*)	$4.46 \cdot 10^{-6}$ (*)	$1.79 \cdot 10^{-7}$ (*)
one-sided test (ALPS-LAB<ALPS-PAS)	$8.87 \cdot 10^{-8}$(*)	$2.23 \cdot 10^{-6}$ (*)	$8.95 \cdot 10^{-8}$(*)
(B)	**Comparison of ROI-options**		
frame	**MNI ROIs – Manual ROIs in DWI space**	**MNI ROIs - MNI ROIs in DWI space**	**Manual ROIs in DWI space - MNI ROIs in DWI space**
LAB (two-sided test)	0.002 (*)	0.026 (*)	0.173
PAS (two-sided test)	0.116	0.009 (*)	1.00

Figure 3: (1) Mean values and standard deviation of DTI-ALPS-indices (ALPS-LAB and ALPS-PAS). (2) Results of paired, two-tailed t-tests. The (*) marks the significant test results below the significance limit of p = 0.05. These correspond to the (*) in (1). Note that there is no significant difference between Manual ROIs in DWI space and MNI ROIs in DWI space in both LAB and PAS.

Comparing the different ROI-options (A, B, C), to select the regions to evaluate the DTI-ALPS-index, we found that the ROI-options B and C were placed in physiologically meaningful locations (SCR and SLF) for all measurements with normal head positioning (Figure 4).

The distance of the centre of mass between the ROI-options B and C was 3.5 mm on average with a standard deviation of approximately 2 mm, with extremes of 0 mm and 10.4. mm (Figure 4).

No statistically significant difference (Figure 3.2B) was found between the indices calculated in the ROI-options B and C ($p = 0.173$ for ALPS-LAB, $p = 1$ ALPS-PAS). For ROI-options A and B, the significance depended on the evaluation method, $p = 0.002$ for ALPS-LAB, 0.116 for ALPS-PAS, as it did for the ROI-options A and C with $p = 0.026$ for ALPS-LAB and $p=0.009$ for ALPS-PAS. Notably, the mean index using ALPS-LAB was smallest for the ROI-option A compared to the other two ROI-options (Supporting Table S1).

The reproducibility of both ALPS-LAB and ALPS-PAS was better for ROI-options A and C compared to ROI-option B, as determined in two test-retest experiments (Supporting Table S1). Similarly, in all ROI-options, ALPS-PAS was more reproducible than ALPS-LAB.

A voluntary rotation of the head resulted in a reduced ALPS-LAB, but ALPS-PAS was less affected (Supporting Table S1).

The matching of the ROI-option C with the ALPS-fibre-regions, for both with and without rotation is shown in Supporting Figure S4. The ratios of the distances of centres of mass in Figure 4 do not behave in a striking pattern, neither regarding the inclusion of head rotation nor regarding the fibre-regions.

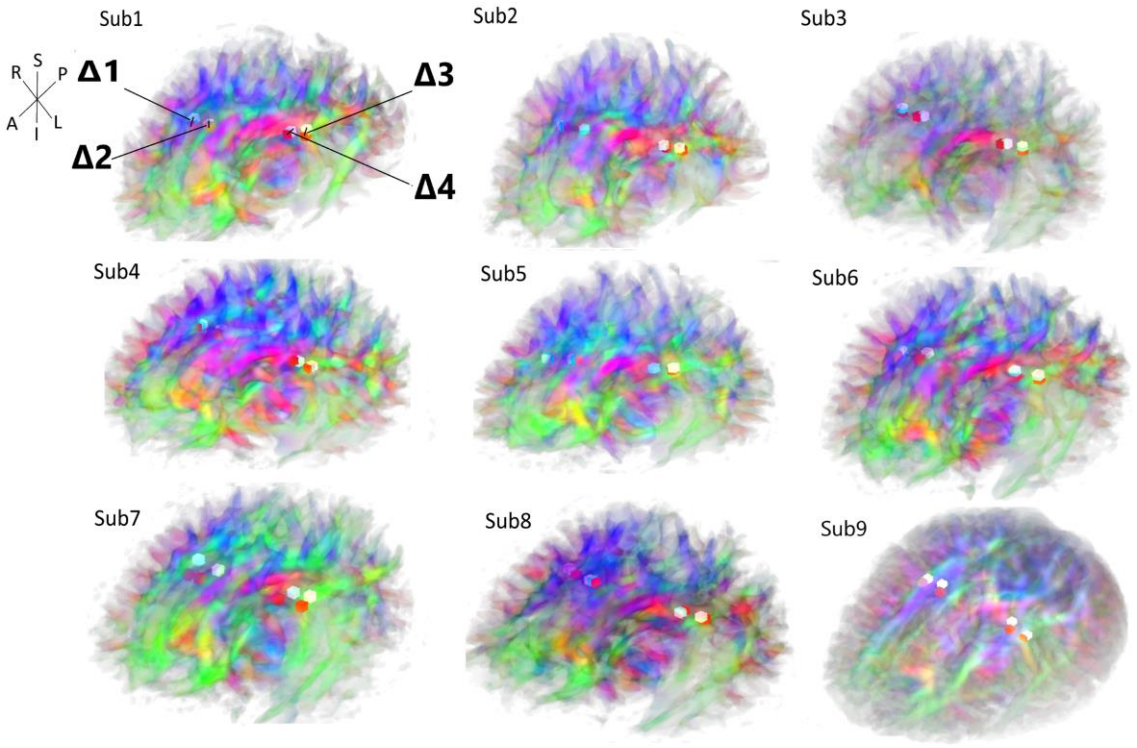

Sub	Δ1 [mm]	Δ2 [mm]	Δ3 [mm]	Δ4 [mm]
Sub 1	2.83; ret: 6.63 (42.6%)	2.83; ret.: 6.32 (44.7%)	2.83; ret.: 2.83 (100%)	2.0; ret.: 4.47 (44.7%)
Sub 2	2.0	0.0	2.83	2.83
Sub 3	2.0; ret.: 2.0 (100%)	2.83; ret.: 2.0 (141.5%)	2.83; ret.: 2.83 (100%)	2.0; ret.: 2.83 (70.67%)
Sub 4	2.0	4.47	4.47	2.0
Sub 5	2.0	2.0	0.0	3.46
Sub 6	4.0	6.0	2.0	2.0
Sub 7	10.39	10.2	10.2	6.32
Sub 8	4.47	2.0	2.0	2.83
Sub 9	2.0; ret.: 8.25 (24.24%)	4.0; ret.: 8.94 (44.74%)	4.9; ret.: 4.0 (122.5%)	4.9; ret.: 6.32 (77.53%)
Mean	3.52	3.81	3.56	3.15
STD	2.59	2.77	2.70	1.44

Figure 4: RGB-encoded maps of diffusion images with manually (red, ROI-option B) and automatically (white, ROI-option C) placed ROIs in the native imaging space (DWI space) for all volunteers. In each region, the distance between the centre of mass for ROI-option B and ROI- option C was calculated (Δ1- Δ4). On average, the distances were about (3.5 ± 2.7) mm, and the DTI-ALPS-indices in these regions were not statistically different (Figure 3). 'ret' is a short-notation for retest and includes the distances as well as the ratio of the test-retest distances in percent.

Lastly, we calculated ALPS-PAS and ALPS-LAB for every voxel of the DWI data, leading to an ALPS-PAS-map and an ALPS-LAB-map (Figure 5). Most parts of the brain showed an anisotropy of the second and third diffusion direction. Differences of up to 100% were observed not only in the ALPS-fibre-regions

(indicated by arrows), but also in deep projection fibres such as the pyramids of the medulla oblongata (Figure 5). These percentage differences were calculated as (second largest diffusivity / third largest diffusivity) – 1, meaning that a 100% difference indicates that the value in one map is twice as high as in the other (e.g., difference values of 1).

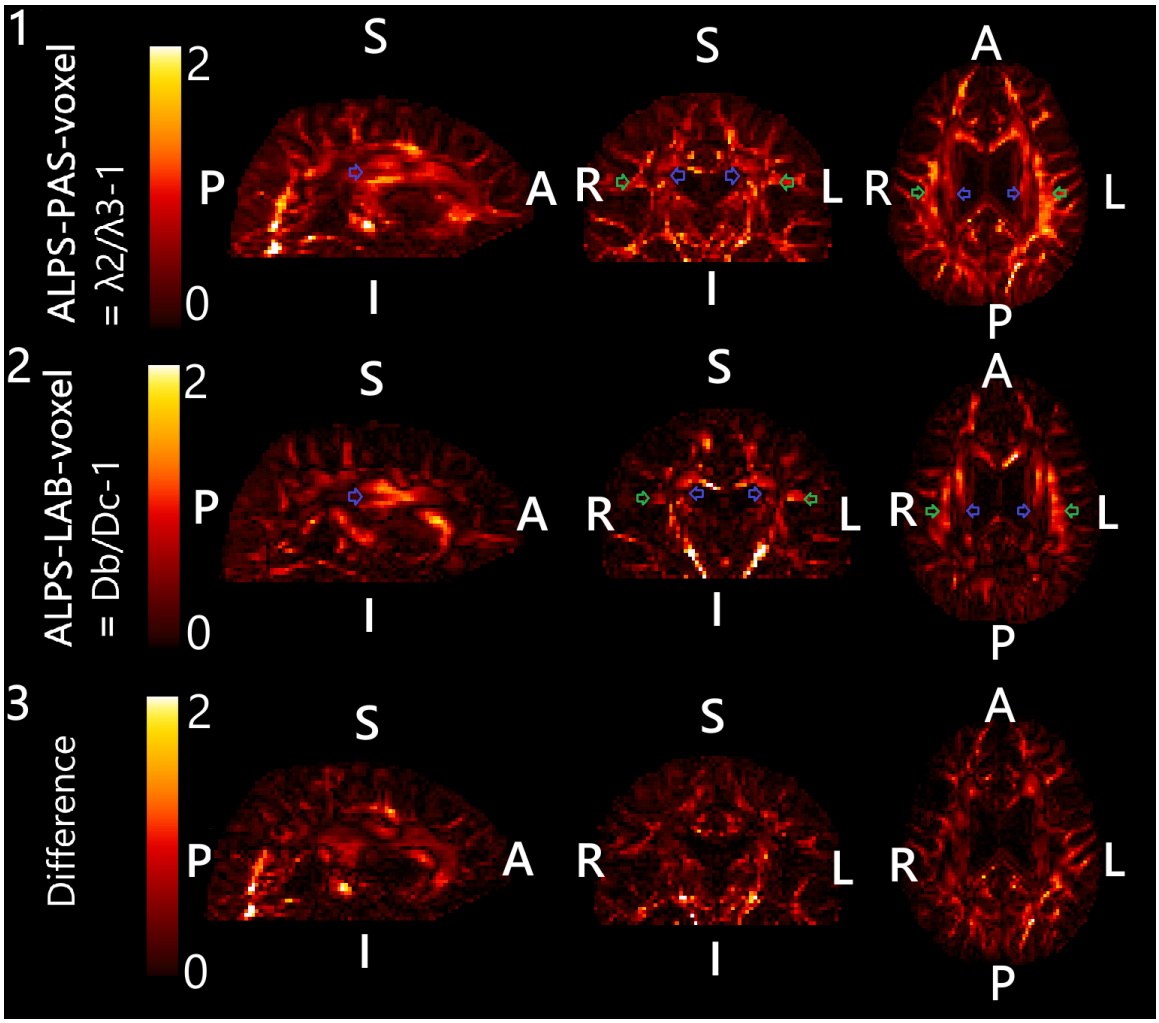

Figure 5: Sagittal, axial and coronal maps of whole-brain ALPS-PAS-voxel (1), ALPS-LAB-voxel (2), and their absolute difference map (3) of a healthy volunteer (Sub9). The classical ALPS-fibre-regions (green and blue arrows) show a high index, as do other regions. Overall, anatomical structures appear better represented on the ALPS-PAS-map.

Discussion

We introduced novel methods to make the DTI-ALPS-index less susceptible to individual head and fibre orientations, less susceptible for individual ROI selection, as well as a method to calculate and visualise a DTI-ALPS-related-index for the entire brain.

Simulating the dependency of the DTI-ALPS-index on rotations indicated that a mismatch between brain anatomy and scanner coordinate system can have a non-negligible impact on the DTI-ALPS-index. These findings were confirmed in vivo, where the DTI-ALPS-index was found to deviate up to 20% depending on the alignment of fibres, described by the Kardan-angles. This effect was apparent in the ROIs in the DWI space (ROI-options B and C), but also after transformation of the data into MNI space (ROI-option A), indicating that this transformation alone may not be enough to correct for varying head and fibre orientations in the brain.

In principle, this variability should be corrected by evaluating DTI-ALPS-index along the principal diffusion directions (ALPS-PAS) instead of the scanner directions. Indeed, the ALPS-PASs were statistically significantly higher than all ALPS-LABs in this study. Likely, this effect can be attributed to fibre-bundles, which are not oriented along the laboratory frame. In addition, test-retest measurements showed higher reproducibility for ALPS-PAS than ALPS-LAB. Thus, ALPS-PAS appears to be more beneficial than ALPS-LAB.

It should be noted, though, that neither ALPS-PAS nor ALPS-LAB necessarily proof the existence of glymphatic flow in PVS, nor the orientation of PVS along the second axis of the PAS. The ALPS-PAS calculation is still based on the DTI approach, which averages all tissue diffusivities into one tensor. This question should be investigated with additional trials in the future. Still, a measurable anisotropy between the second and third principal diffusion direction exists, not only in the classical ALPS-fibre-regions, but as well, when calculated voxel-wise, in many other regions of the brain (Figure 5). These maps may suggest more regions where DTI-ALPS can be evaluated.

Manual placement of the ROIs (ROI-option B) is operator depended on and thus another source of variability. Using standardised, atlas-based ROIs (ROI-option C) appears to be a suitable solution, but requires either transforming the images to an atlas, or the atlas-based ROIs to the native images.

Evaluating the DTI-ALPS-index in the MNI space, compared to DWI space, reduced the mean value and thus the measured DTI-ALPS effect or "secondary anisotropy" significantly for ALPS-LAB. Using PAS reduced the effect so that the difference was no longer statistically significant. These findings may be explained by the fact that transforming the DWI data to an atlas space (here: MNI) is a quite invasive operation, where many anatomical features and thus fibre orientations are altered (Figure 1C). Using the PAS appears to compensate for this effect partially.

Transforming the atlas-based ROIs to the native imaging (DWI) space did not significantly change the indices, neither for PAS nor LAB. Here, the mean distance between the manually placed and automatically placed ROIs was about 3 mm.

These findings suggest that it is beneficial (with respect to effect size) to calculate the DTI-ALPS-index in the native imaging space on standardised ROIs (that were transformed into the space from an atlas (ROI-option C)), rather than to transform the whole imaging data to the atlas space (where the standardised ROIs were defined (ROI-option A)). The conducted test-retest measurements support this idea. Thus, calculating the DTI-ALPS-index in standardised ROIs transformed from an atlas in the imaging space may allow to reduce operator variability.

The voxel-wise calculation of DTI-ALPS offers an interesting approach to evaluate and visualise DTI-ALPS not only in selected regions, but the entire brain. Here, the classical ALPS-fibre-regions as well as other areas showed a strong secondary anisotropy. Notably, anatomical features were subjectively much more consistent for PAS than for LAB. Whether or not the DTI-ALPS-index is of interest has to be evaluated and remains to be seen.

Conclusion

Using the principal diffusion directions (PAS) instead of the scanner directions (LAB) to calculate the DTI-ALPS-index increased its value by up to 20% in this study. Evaluating both indices (ALPS-LAB and ALPS-PAS) in standardised ROIs transformed from an atlas to the imaging space was not found to be inferior to manual ROI placement but eliminates potential inter-operator variability. Together, both ALPS-PAS and standardised ROIs increased the DTI-ALPS effect and made it more robust. Whole brain ALPS-LAB-map and ALPS-PAS-map show interesting features which will have to be investigated separately.

ACKNOWLEDGMENTS

We sincerely thank Dr. Thorsten Feiweier for reviewing this paper and providing valuable and constructive feedback that helped improve the final version.

Financial disclosure

None reported.

Conflict of interest

The authors declare no potential conflict of interests. Ali Ajouz is an employee of Siemens Healthineers AG and UKSH.

Supporting information

Subjects	Side	MNI ROIs		Manual ROIs in DWI (volunteer) space		MNI ROIs in DWI (volunteer) space	
		ALPS-LAB	ALPS-PAS	ALPS-LAB	ALPS-PAS	ALPS-LAB	ALPS-PAS
Sub1 (f, 24)	L Retest ratio	1.60 1.40 114.3%	1.82 1.83 99.5%	1.71 1.32 129.5%	1.93 1.52 126.9%	1.70 1.34 126.9%	1.94 1.71 113.4%
	R Retest ratio	1.61 1.53 105.2%	1.72 1.71 100.5%	1.68 1.82 92.3%	1.72 1.69 101.7%	1.54 1.44 106.9%	1.71 1.65 103.6%
Sub2 (m, 29)	L	1.49	1.64	1.72	1.88	1.50	1.62
	R	1.55	1.65	1.60	1.70	1.64	1.75
Sub3 (m, 27)	L Retest ratio	1.56 1.56 100%	1.72 1.73 99.4%	1.63 1.59 102.5%	1.76 1.73 101.7%	1.64 1.64 100%	1.79 1.80 99.4%
	R Retest ratio	1.36 1.36 100%	1.43 1.44 99.3%	1.28 1.49 85.9%	1.35 1.59 84.9%	1.41 1.37 102.9%	1.46 1.46 100%
Sub4 (f, 23)	L	1.62	1.85	1.69	1.83	1.69	1.92
	R	1.55	1.63	1.62	1.63	1.59	1.68
Sub5 (m, 27)	L	1.51	1.72	1.60	1.78	1.67	1.86
	R	1.41	1.48	1.56	1.60	1.35	1.40
Sub6 (f, 49)	L	1.55	1.97	1.71	2.14	1.51	1.96
	R	1.71	1.85	1.71	1.90	1.73	1.90
Sub7 (f, 26)	L	1.39	1.74	1.53	1.73	1.42	1.71
	R	1.33	1.53	1.35	1.41	1.43	1.60
Sub8 (f, 26)	L	1.50	1.68	1.42	1.63	1.52	1.72
	R	1.56	1.75	1.54	1.67	1.57	1.80
Sub9 (f, 30)	L Retest ratio	1.39 1.40 99.2%	1.65 1.65 100%	1.46 1.61 90.7%	1.66 1.78 93.2%	1.37 1.42 96.4%	1.64 1.64 100%
	R Retest ratio	1.34 1.30 103.1%	1.52 1.51 100.6%	1.51 1.80 83.9%	1.74 1.96 88.8%	1.37 1.32 103.8%	1.60 1.49 107.4%
Mean	L	1.51	1.75	1.61	1.82	1.56	1.80
	R	1.49	1.62	1.54	1.64	1.51	1.66
Relative mean [%]	L	100	116	100	113	100	115
	R	100	109	100	106	100	110
CV (relative to mean) [%]	L	5.10	5.76	6.68	8.07	7.36	6.84
	R	8.55	8.10	8.76	9.71	8.17	9.07

Supporting Table S1: For both, DWI (Manual ROIs in DWI (volunteer) space, MNI ROIs in DWI (volunteer) space) and MNI (atlas) space, the DTI-ALPS-index is calculated in the laboratory frame (ALPS-LAB) and in the principal axis system (ALPS-PAS) for each brain side (Left-L, Right-R). Subject information is given in the first column including the gender (female-f, male-m) and age in years. For subjects one, three and nine, ALPS-indices of a retest measurement are represented in an additional line for each brain hemisphere. The line 'ratio' defines the test-index divided by the retest-index in percent. In addition, the mean, relative mean and the coefficient of variance (CV) across subjects, excluding the retest-measurements, are included.

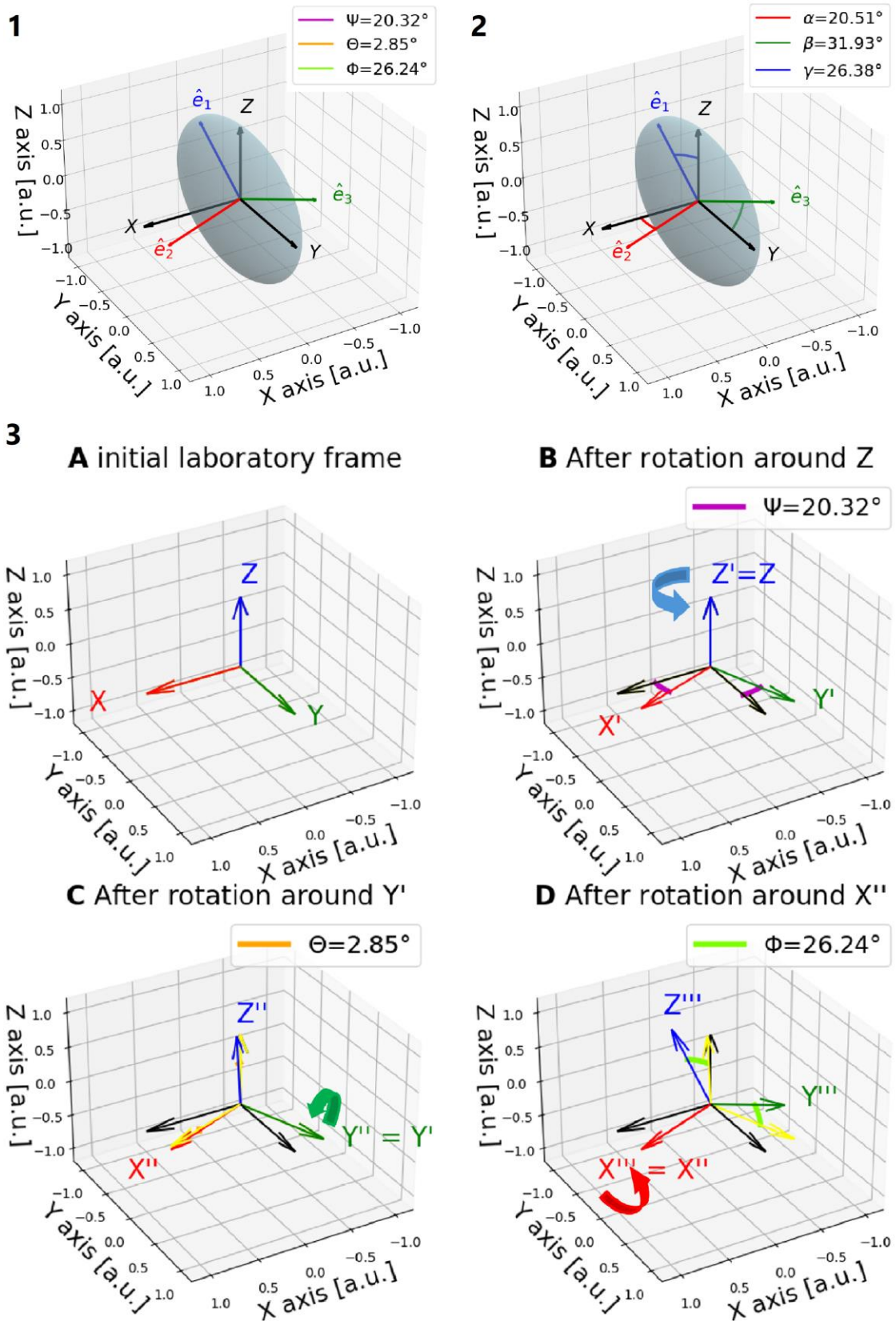
1
Ψ=20.32°
Θ=2.85°
Φ=26.24°
2
α=20.51°
β=31.93°
γ=26.38°
3
A initial laboratory frame
B After rotation around Z
C After rotation around Y'
D After rotation around X''
Z axis [a.u.]
Y axis [a.u.]
X axis [a.u.]
Z
X
Y
Z'=Z
X'
Y'
Z''
X''
Y'' = Y'
Z'''
X''' = X''
Y'''

Supporting Figure S1: Illustration of an exemplary diffusion tensor from a voxel in the SCR area of a volunteer with eigenvalues in [µm²/ms] $\lambda_1 = 1.06, \lambda_2 = 0.54, \lambda_3 = 0.35$ and eigenvectors $\hat{e}_1$ = (-0.93, -0.34, 0.04)^T, $\hat{e}_2$ = (0.29, -0.84, -0.44)^T, $\hat{e}_3$= (-0.19, 0.39, -0.89)^T. The transformation between the Cartesian laboratory axes and the eigenvectors (or principal axis) of the diffusion tensor can be described by three subsequent Kardan-rotations Z, Y', X'' (3a-c). The minimal (absolute) angels between the PAS and laboratory frame are shown in 2).

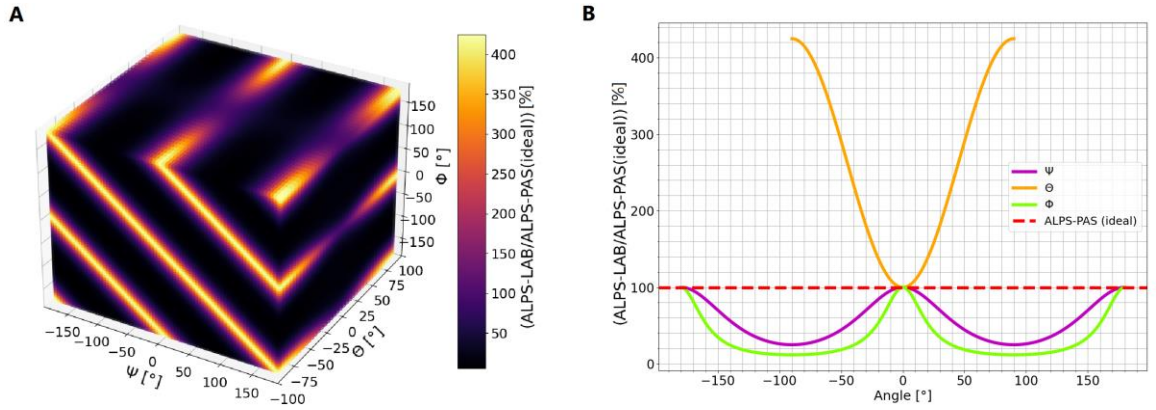

Supporting Figure S2: (A) In addition to Figure 3.1, the relation of ALPS-LAB to ALPS-PAS for multiple Kardan-angle combinations with a simultaneous change of all angles is plotted. (B) Similar to (A) but setting two Kardan-angles to zero while varying the third in the entire Kardan-angle range.

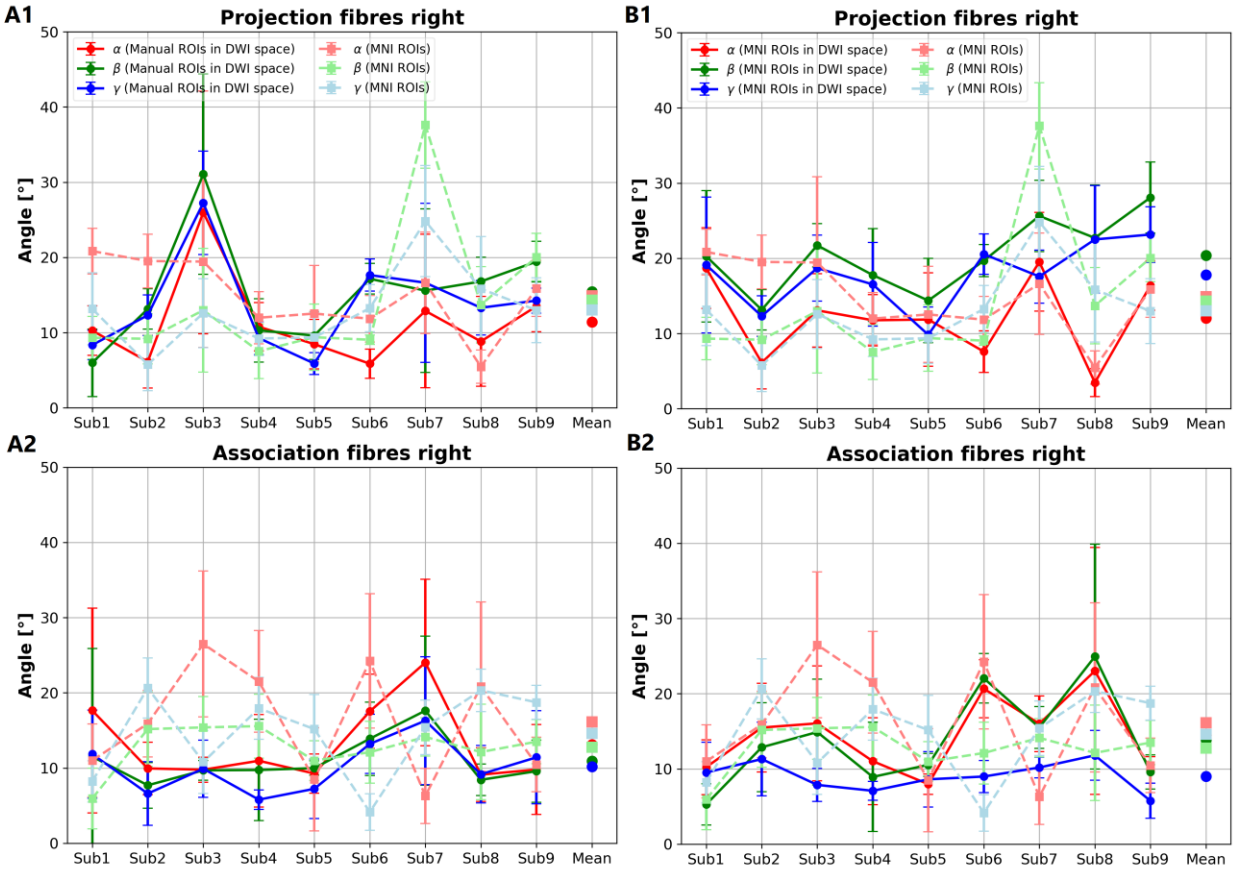

Supporting Figure S3: The curves represent the mean and standard deviation values of the three absolute angles computed for each voxel within the ROIs, which are defined per ALPS-fibre-region. For each angle, the mean and standard deviation were calculated across voxels within each ROI for each subject. Subsequently, these values were averaged across subjects. The results shown are for the right hemisphere as an illustration. The colours blue, green and red characterize($\boldsymbol{\alpha}, \boldsymbol{\beta}, \boldsymbol{\gamma}$) in DWI space (A1,2: Manual ROIs in DWI space; B1,2: MNI ROIs in DWI space) and light blue, light green and light purple characterize ($\boldsymbol{\alpha}, \boldsymbol{\beta}, \boldsymbol{\gamma}$) in MNI space (MNI ROIs).

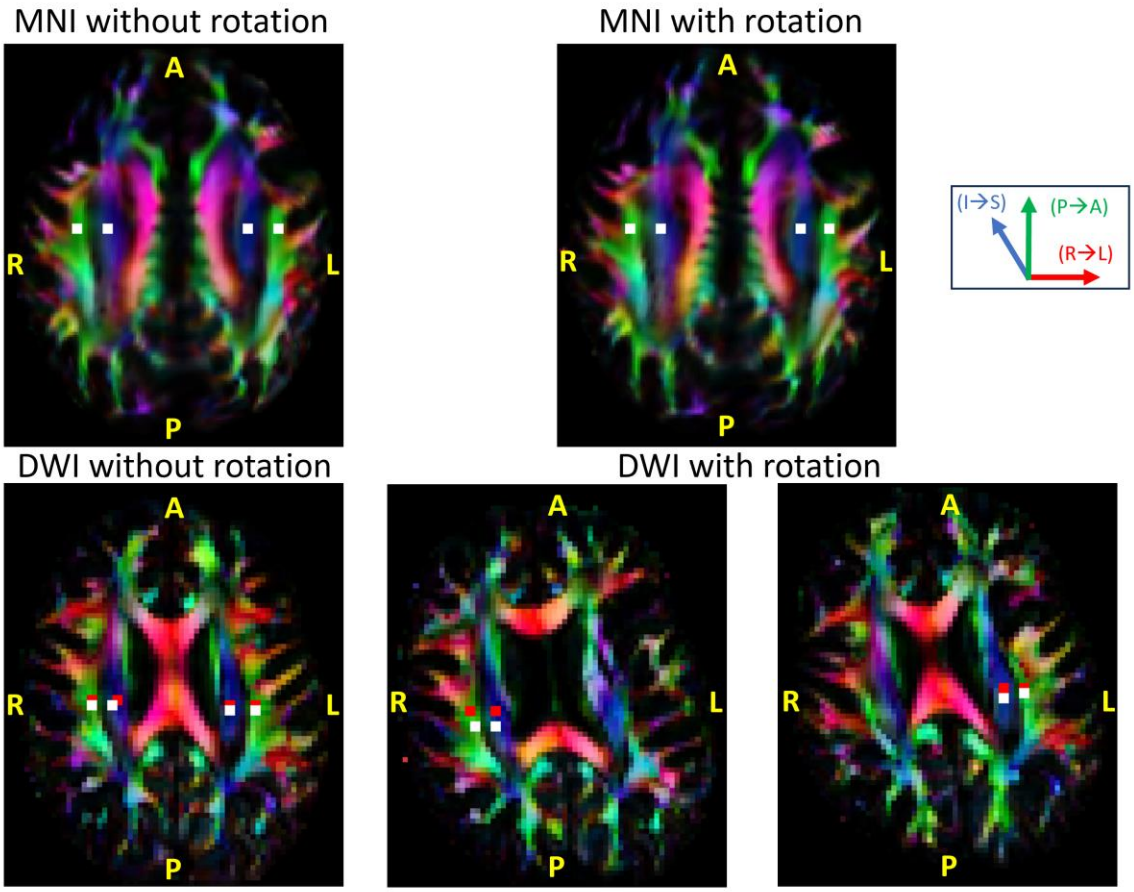

Supporting Figure S4: Exemplary RGB maps in MNI space (upper) with MNI ROIs (white squares ROI-option A) and in DWI space (down) with Manual ROIs in DWI space (red squares ROI-option B) and MNI ROIs in DWI space (white squares ROI-option C) of subject one, with (right) and without (left) head rotation. In all cases, the algorithm placed the ROIs (ROI-option C) in anatomically meaningful areas (green and blue areas). Note the smoothing effect of transforming the data to the MNI space.

ORCID

Ali Ajouz 0009-0006-2251-0361

Olav Jansen 0000-0002-7330-1942

Lynn Johann Frohwein 0000-0003-3474-115X

Svea Seehafer 0009-0001-2573-5770

Naomi Larsen 0000-0002-8782-8278

Jan-Bernd Hövener 0000-0001-7255-7252

References

1. Iliff JJ, Wang M, Liao Y, et al. A Paravascular Pathway Facilitates CSF Flow Through the Brain Parenchyma and the Clearance of Interstitial Solutes, Including Amyloid β. *Sci Transl Med*. 2012;4(147). doi:10.1126/scitranslmed.3003748

2. Bohr T, Hjorth PG, Holst SC, et al. The glymphatic system: Current understanding and modeling. *iScience*. 2022;25(9):104987. doi:10.1016/j.isci.2022.104987

3. Smith AJ, Verkman AS. The "glymphatic" mechanism for solute clearance in Alzheimer's disease: game changer or unproven speculation? *FASEB j*. 2018;32(2):543-551. doi:10.1096/fj.201700999

4. Kamagata K, Saito Y, Andica C, et al. Noninvasive Magnetic Resonance Imaging Measures of Glymphatic System Activity. *Magnetic Resonance Imaging*. 2024;59(5):1476-1493. doi:10.1002/jmri.28977

5. Taoka T, Naganawa S. Glymphatic imaging using MRI. *Magnetic Resonance Imaging*. 2020;51(1):11-24. doi:10.1002/jmri.26892

6. Joseph CR, Benhatzel CM, Stern LJ, Hopper OM, Lockwood MD. Pilot study utilizing MRI 3D TGSE PASL (arterial spin labeling) differentiating clearance rates of labeled protons in the CNS of patients with early Alzheimer disease from normal subjects. *Magn Reson Mater Phy*. 2020;33(4):559-568. doi:10.1007/s10334-019-00818-3

7. Chen Y, Dai Z, Fan R, et al. Glymphatic System Visualized by Chemical-Exchange-Saturation-Transfer Magnetic Resonance Imaging. *ACS Chem Neurosci*. 2020;11(13):1978-1984. doi:10.1021/acschemneuro.0c00222

8. Gomolka RS, Hablitz LM, Mestre H, et al. Loss of aquaporin-4 results in glymphatic system dysfunction via brain-wide interstitial fluid stagnation. *eLife*. 2023;12:e82232. doi:10.7554/eLife.82232

9. Taoka T, Masutani Y, Kawai H, et al. Evaluation of glymphatic system activity with the diffusion MR technique: diffusion tensor image analysis along the perivascular space

(DTI-ALPS) in Alzheimer's disease cases. *Jpn J Radiol*. 2017;35(4):172-178. doi:10.1007/s11604-017-0617-z

10. Taoka T, Ito R, Nakamichi R, et al. Reproducibility of diffusion tensor image analysis along the perivascular space (DTI-ALPS) for evaluating interstitial fluid diffusivity and glymphatic function: CHanges in Alps index on Multiple conditiON acquIsition eXperiment (CHAMONIX) study. *Jpn J Radiol*. 2022;40(2):147-158. doi:10.1007/s11604-021-01187-5

11. Taoka T, Ito R, Nakamichi R, Nakane T, Kawai H, Naganawa S. Diffusion Tensor Image Analysis ALong the Perivascular Space (DTI-ALPS): Revisiting the Meaning and Significance of the Method. *MRMS*. 2024;23(3):268-290. doi:10.2463/mrms.rev.2023-0175

12. Tatekawa H, Matsushita S, Ueda D, et al. Improved reproducibility of diffusion tensor image analysis along the perivascular space (DTI-ALPS) index: an analysis of reorientation technique of the OASIS-3 dataset. *Jpn J Radiol*. 2023;41(4):393-400. doi:10.1007/s11604-022-01370-2

13. Saito Y, Kamagata K, Andica C, et al. Reproducibility of automated calculation technique for diffusion tensor image analysis along the perivascular space. *Jpn J Radiol*. 2023;41(9):947-954. doi:10.1007/s11604-023-01415-0

14. Ajouz A. Impact of image registration and fibre orientation on the DTI-ALPS-index. In: *26th Ann. Meet. Ger. Chapter Int. Soc. Magn. Reson. Med. 2024, Tübingen*. Tübingen, Germany; 2024:129-130. doi:https://plan.events.mpg.de/event/204/overview

15. Ajouz A. Using a principle axis system allows automatic evaluation of glymphatic flow with ALPS in imaging space and corrects for head and fibre orientation. In: *2025 ISMRM & ISMRT Annual Meeting & Exhibition*. Honolulu, Hawai'i, USA; 2025. https://www.ismrm.org/25/accepted_abstracts.pdf.

16. Jenkinson M, Beckmann CF, Behrens TEJ, Woolrich MW, Smith SM. FSL. *NeuroImage*. 2012;62(2):782-790. doi:10.1016/j.neuroimage.2011.09.015

17. Basser PJ, Mattiello J, LeBihan D. MR diffusion tensor spectroscopy and imaging. *Biophysical Journal*. 1994;66(1):259-267. doi:10.1016/S0006-3495(94)80775-1

18. Yang F, Zhu YM, Kingsley PB. A further investigation of the Euler angle calculation in diffusion tensor imaging. In: *2016 IEEE 13th International Conference on Signal Processing (ICSP)*. Chengdu, China: IEEE; 2016:39-43. doi:10.1109/ICSP.2016.7877792

19. Avants B, Tustison NJ, Song G. Advanced Normalization Tools: V1.0. *The Insight Journal*. July 2009. doi:10.54294/uvnhin

20. Tournier JD, Smith R, Raffelt D, et al. MRtrix3: A fast, flexible and open software framework for medical image processing and visualisation. *NeuroImage*. 2019;202:116137. doi:10.1016/j.neuroimage.2019.116137

21. Garyfallidis E, Brett M, Amirbekian B, et al. Dipy, a library for the analysis of diffusion MRI data. *Front Neuroinform*. 2014;8. doi:10.3389/fninf.2014.00008

22. Mori S, Oishi K, Jiang H, et al. Stereotaxic white matter atlas based on diffusion tensor imaging in an ICBM template. *NeuroImage*. 2008;40(2):570-582. doi:10.1016/j.neuroimage.2007.12.035

23. Hua K, Zhang J, Wakana S, et al. Tract probability maps in stereotaxic spaces: Analyses of white matter anatomy and tract-specific quantification. *NeuroImage*. 2008;39(1):336-347. doi:10.1016/j.neuroimage.2007.07.053

24. Wakana S, Caprihan A, Panzenboeck MM, et al. Reproducibility of quantitative tractography methods applied to cerebral white matter. *NeuroImage*. 2007;36(3):630-644. doi:10.1016/j.neuroimage.2007.02.049